Effect of Surface Roughness on Boundary Layer Transition and Far Field Noise

Ye, Qingqing; Avallone, Francesco; Ragni, Daniele; Choudhari, Meelan; Casalino, Damiano

DOI
10.2514/6.2019-2551

Publication date
2019

Document Version
Final published version

Published in
25th AIAA/CEAS Aeroacoustics Conference

Aeroacoustics Conferences
20-23 May 2019, Delft, The Netherlands
25th AIAA/CEAS Aeroacoustics Conference

10.2514/6.2019-2551

Effect of Surface Roughness on Boundary Layer Transition and Far Field Noise

Qingqing Ye,[1] Francesco Avallone,[2] Daniele Ragni,[3]
Delft University of Technology, Delft, 2629HS, The Netherlands

Meelan Choudhari,[4]
NASA Langley Research Center, Hampton, VA 23681, U.S.A.

and
Damiano Casalino[5]
Delft University of Technology, Delft, 2629HS, The Netherlands

Surface roughness elements are often used to force laminar to turbulent transition during aerodynamic and aeroacoustic experiments in wind tunnels. The statistical features and frequency content of the forced turbulent boundary layer can influence the far-field trailing edge noise. To study this dependence, boundary layer transition induced by randomly distributed roughness elements and a zigzag strip of the same height over a NACA 0012 airfoil is investigated experimentally. The effects of roughness type on the near-field flow topology, transition location, and far-field noise are addressed. At a fixed roughness height, the distributed roughness elements are less effective in forcing transition than the zigzag trip at low freestream velocity (u_∞ < 20 m/s). As u_∞ increases, the transition front for the distributed roughness elements moves close to the roughness location, reaching the same or even further upstream location compared with the zigzag strip. The far-field noise intensity depends on the transition location. For u_∞ < 20 m/s, a higher noise level is measured for the distributed roughness with respect to the zigzag strip. Whereas, for $u_\infty \geq$ 20m/s, the earlier onset of transition leads to a lower noise level for the distributed roughness elements with respect to the zigzag strip. The data confirms that an adequate characterization of the state of the boundary layer is necessary when measuring far-field noise in wind tunnel experiments.

I. Nomenclature

b	=	span of the airfoil model
c	=	chord of the airfoil model
f	=	frequency
H	=	shape factor
L_p	=	1/3-octave band sound pressure level (ref 20 μPa)
M_∞	=	freestream Mach number
R	=	reference observer distance
Re_c	=	chord-based Reynolds number
St	=	Strouhal number
t	=	recording time
u_∞	=	freestream velocity

[1] Postdoc Researcher, Department of Aerodynamic, Wind Energy and Propulsion, q.ye-1@tudelft.nl.
[2] Assistant Professor, Department of Aerodynamic, Wind Energy and Propulsion, f.avallone@tudelft.nl, AIAA Member.
[3] Assistant Professor, Department of Aerodynamic, Wind Energy and Propulsion, d.ragni@tudelft.nl, AIAA Member.
[4] Aerospace Technologist, Meelan.M.Choudhari@nasa.gov, AIAA Fellow.
[5] Full Professor, Department of Aerodynamic, Wind Energy and Propulsion, d.casalino@tudelft.nl, AIAA Member.

u' = streamwise velocity fluctuations
x = Cartesian coordinate axes aligned with the airfoil chord
x_t = chordwise location of transition front
y = Cartesian coordinate axes normal to airfoil chord and span
z = Cartesian coordinate axes aligned with the airfoil span
δ_{99} = boundary layer thickness
δ^* = displacement thickness
θ = momentum thickness
v = kinematic viscosity
$< >$ = root mean square (RMS)
Δ = value difference

II. Introduction

The aerodynamic noise generated by the convection of a turbulent boundary layer past the trailing edge is a dominant noise source for wind turbines [1]. The intensity of the far-field noise and its spectral distribution is strongly dependent on the boundary layer properties at the trailing edge, which can be affected by the onset location of transition. Uncertainty in the transition location has an effect on the comparison between experiments carried out in different wind tunnels, which may differ in the intensity of freestream turbulence or in the way the process of laminar-turbulent transition is induced in the boundary layer flow. Herr et al. [2] provide a partial overview of representative numerical simulations and their comparison with available measurements of trailing edge noise for both symmetric and cambered airfoils within the framework of the BANC series of workshops hosted by the AIAA [3].

Boundary layer trips used to force transition are usually divided into two main categories: two-dimensional roughness elements (e.g., wires, steps, and gaps) and three-dimensional roughness elements (e.g., isolated or distributed roughness elements). Two-dimensional boundary layer trips influence the transition process via enhanced amplification of Tollmien-Schlichting (TS) waves, especially within the separation and recovery region behind the roughness [4]. An increase of the Reynolds number based on the roughness height leads to larger growth of the TS wave amplitude [5], resulting in a gradual upstream shift of the transition location toward the location of the roughness element [6]. Three-dimensional roughness elements induce a localized spanwise deflection of the boundary layer flow. Counterrotating streamwise vortex pairs are produced in the roughness wake [7, 8], resulting in the formation of low- and high-speed streaks, which modulate the surface shear along the spanwise direction Once the streak amplitude exceeds a critical value, the streak will be subject to a secondary instability in the form of either sinuous or varicose modulation that eventually leads to a breakdown to turbulence [9].

Compared with isolated roughness elements, distributed roughness elements are more widely used as tripping devices for wind-turbines blades and airfoils due to their higher tripping efficiency and improved spanwise uniformity of the downstream turbulent flow [10-13]. Wind-turbine blades also suffer from erosion caused by sand or hail, insect deposits, and icing, resulting in the formation of similarly rough surfaces close to the leading edge, which also influences the boundary layer properties [14]. To avoid the sensitivity of airfoil self-noise to transition location during wind tunnel experiments at low Reynolds numbers, oversized boundary layer trips are often used to ensure a fully turbulent boundary layer at the trailing edge [15]. However, the excessive trip may introduce coherent flow structures that can persist up to the trailing edge, thus altering the streamwise and spanwise correlations of a turbulent boundary layer. As a result, a good understanding of the transition mechanism is necessary to provide guidelines for transition prediction and the parameter selection for the boundary layer trip.

Acoustic measurements with microphone arrays have been used in recent years to investigate the effect of surface roughness on trailing edge noise. Hutcheson and Brooks [11] measured the trailing edge noise from an NACA 63-215 airfoil, where the boundary layer was tripped with steel grits of 0.29 mm diameter over the first 5% of the chord. It was found that trailing edge noise is the dominant noise source in the low frequency range. On the other hand, the scrubbing type of noise close to the leading edge becomes the dominant contributor at high frequencies due to the presence of surface roughness. Cheng et al. [13] investigated the effect of roughness induced by surface icing on the broadband noise due to rotors. The height of surface roughness changes both the boundary layer thickness and the turbulent intensity at the trailing edge. The increase of the latter strongly affects the trailing edge noise, leading to a significant noise increase at high frequencies. For a full-scale wind turbine, Oerlemans et al. [1] performed acoustic measurements to detect the dominant noise sources. When the blade is overtripped with large sized roughness elements, the noise level and source area were found to increase significantly.

Until recently, the research on distributed surface roughness effect on boundary layer transition did not devote enough attention to identifying the correlation between flow topology, transition mechanism, and far-field noise. The present research aims to further the current understanding on these aspects via a deeper characterization of the flow field in the context of similar measurements as the classic ones by Brooks et al. [12]. Randomly distributed roughness elements are placed on an NACA 0012 airfoil at zero degrees angle of attack. In experimental measurements of airfoil self-noise, zigzag strips are widely used as three-dimensional boundary layer tripping devices [16, 17]. Thus, for comparison, a zigzag strip with the same height and streamwise length as the distributed roughness patch is also tested. The distribution of the surface roughness is measured via a three-dimensional laser scanner, providing a reference geometry for future numerical study. Infrared thermography is used to measure the surface temperature, enabling the detection of the transition location. The flow field around and downstream of the roughness element is measured by hotwire anemometry. The noise sources are detected by the microphone arrays to highlight the influence of different roughness configurations on the far-field noise.

III. Experimental Setup and Measurement Techniques

A. Flow Conditions and Test Facilities

The experiments were performed in the anechoic vertical open-jet wind tunnel of the Aerodynamics Laboratories of the Aerospace Engineering Faculty at Delft University of Technology. The wind tunnel test section is 0.4×0.7 m^2, which follows a contraction ratio of 15:1. The maximum operating velocity is 42.5 m/s. The turbulence intensity at this velocity is below 0.1%. The freestream velocity distribution across the test section has a uniformity of 0.5%.

An NACA 0012 airfoil with 300 mm chord (c) and 400 mm span (b) was installed between side plates in the symmetry plane of the test section, covering the entire span. The airfoil was set at zero degrees angle of attack. A Cartesian system of coordinate axes centered at the leading edge of the airfoil is introduced, such that the x-axis is aligned with the airfoil chord, the z-axis is along the span, and the y-axis is normal to both of them to form a right handed reference system. The conceptual sketch of the model arrangement is shown in Fig. 1.

Two tripping devices were tested: randomly distributed roughness elements and a zigzag strip. The roughness elements were installed over the chordwise range of x/c = [0.14, 0.18] on both suction and pressure sides of the airfoil over the entire span. The distributed roughness elements have spherical shape (referred to as grit) with a nominal diameter of 0.3 ± 0.1 mm. The density of the roughness elements is approximately 2 elements per mm. The roughness distribution was measured with a high-speed laser scanner (Micro-Epsilon scanCONTROL 2925, max frequency 2 kHz). The laser sheet produced by the scanner intersects with the top half of the spherical grits. As a result, the roughness elements are identified with a hemispherical shape. The range of focus in the wall-normal direction (y) extends up to 26 mm, covering the variation of the wall position. The laser sheet with a length of 29 mm was aligned in the streamwise direction, with 1280 points captured in a single streamwise profile. The spanwise surface variation was measured by moving the scanner with an in-house traverse control system with a step size of 0.025 mm in the range of z/c = [-0.08 0.08]. The scanning resolution in x, y and z are 22, 2, and 25 µm respectively. The scanned surfaces on the suction and pressure sides are shown in Fig. 2. For ease of comparison, a conventional zigzag trip with the same height of 0.3 mm and streamwise extent of $0.04c$ was selected. The top angle of the zigzag trip is 60°.

Experiments were performed at six freestream velocities (u_∞ = 16, 18, 20, 25, 30, and 35 m/s). The corresponding chord-based Reynolds number ($Re_c = u_\infty c/\nu$) varies from 3.29×10^5 to 7.20×10^6. The detailed test conditions are summarized in Table 1.

Table 1. Test conditions

u_∞ (m/s)	16	18	20	25	30	35
Re_c	3.29×10^5	3.7×10^5	4.11×10^5	5.14×10^5	6.17×10^5	7.20×10^5

B. Infrared Thermography

InfraRed (IR) thermography measurements were carried out with an Optris PI640 IR system. The camera has a focal-plane array (FPA) detector with a sensitivity of 75 mK. The sensor size of the camera is 640×480 pixels. The spectral response of the sensor falls in the range of 7.5–13 µm. An objective with a focal length of 41.5 mm was mounted on the IR camera. The recording rate was 30 Hz at full resolution. The measurement domain captured the full airfoil model. The resultant spatial resolution is 2.19 pixels/mm. The camera was mounted at an angle of approximately 20° with respect to the symmetry plane of the tunnel. In order to increase the temperature difference

with the flow, the surface of the model is heated with a high-power daylight lamp. The IR camera is shielded with an aluminium foil to avoid heat radiation from the lamp. As the measured surface temperature distributions are used to extract the transition location, the emissivity and reflectivity are not further corrected.

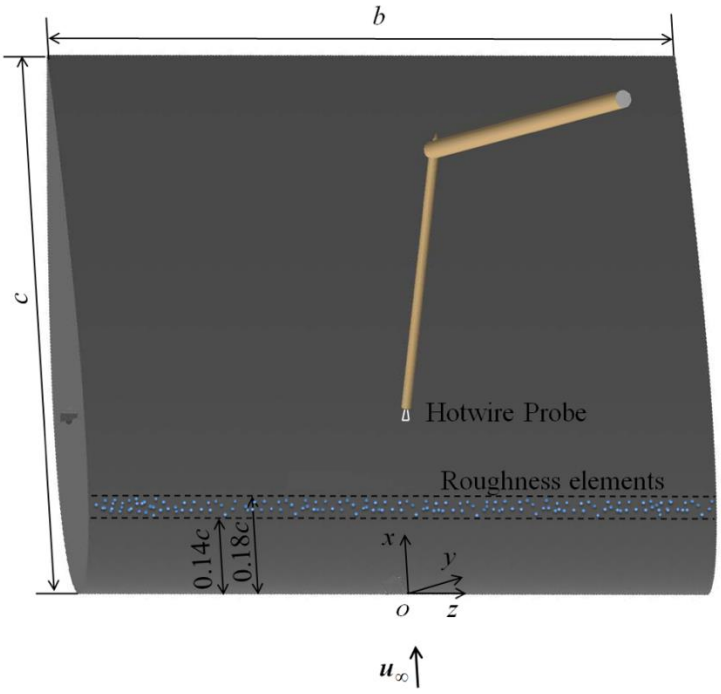

Fig. 1. Sketch of the experimental configuration.

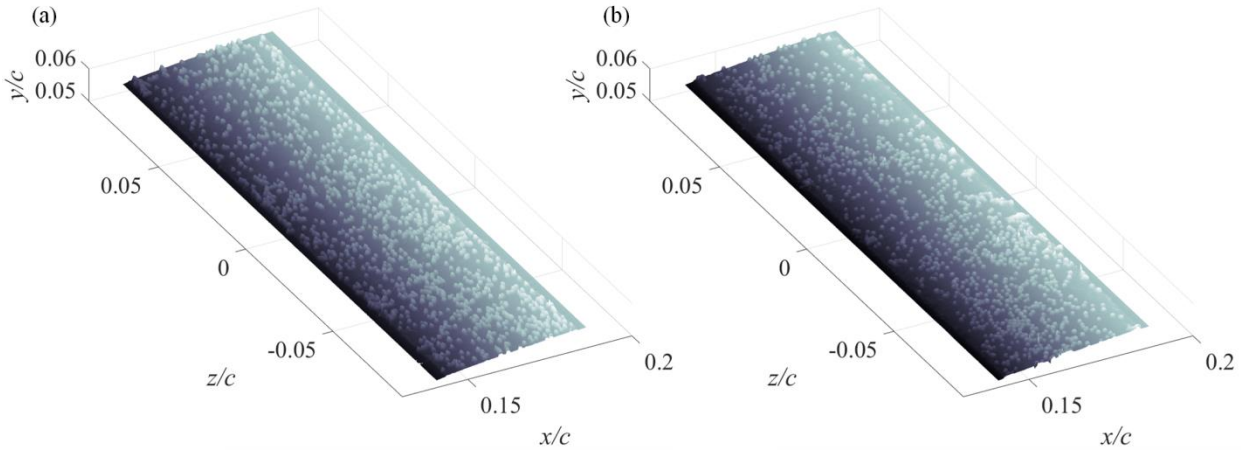

Fig. 2. Reconstructed surface roughness distribution by 3D scanning on the (a) suction and (b) pressure side.

C. Hotwire Anemometry

Hotwire anemometry measurements were carried out to capture the velocity field behind the roughness elements (Fig. 1). A 5 µm diameter single-wire probe (Dantec Dynamics P11) was used in conjunction with a constant temperature bridge (TSI IFA-300). The development of the flow field was measured in *y*-*z* cross-planes at four streamwise positions (x/c = [0.16, 0.19, 0.24, 0.29]), including both directly above the middle of the roughness strip and their near wake. The spanwise extent of the measurement planes is z/c = [-0.08, 0.08] and [-0.08, 0.00] for randomly distributed roughness and the zigzag trip, respectively. For the latter, four spanwise wavelengths are captured in the measurement planes. The trailing edge boundary layer properties were measured at x/c = 0.95 for a spanwise range of z/c = [-0.08, 0.00]. The wall-normal depth of the measurement planes is adapted at each location, depending on the boundary layer thickness. The change of wall location at different streamwise positions is also

taken into consideration. Around 30 points were measured to capture the boundary layer profile. The movement of the hotwire probe is controlled by an in-house traverse system with three-degrees of freedom. The spanwise step size is 1 mm (0.003c). The wall-normal steps vary from point to point depending on the local velocity gradient. The measurement data were acquired at a sampling frequency of 50 kHz. A low-pass filter was applied with a cut-off frequency of 20 kHz. A measurement duration of 2 s was used at each point, ensuring good statistical convergence of the targeted flow statistics.

D. Acoustics Measurement

The location and amplitude of the acoustic sources were measured using a phased microphone array with 64 G.R.A.S. 40PH free-field microphones (frequency response: ±1 dB, frequency range: 10 Hz to 20 kHz, max. output: 135 dB at ref. 2×10^{-5} Pa). The microphones are equipped with CCP preamplifiers to measure the far-field noise emission from the airfoil trailing edge in the presence of both the distributed roughness elements and the zigzag trip. The plane of the microphones array is parallel to the chord center plane of the model at zero degrees angle of attack, with a distance (R) of 1.30 m between the two planes. The microphone placement follows an optimized array distribution with 9 spiral arms [18] and 7 microphones along each arm. Close to the center of the array, an extra microphone is added. The microphone array has an effective extent of 2 m in the streamwise direction and 1 m in the spanwise direction. A sketch of the microphone array distribution is shown in Fig. 3(a).

Measurements were recorded at a sampling frequency of 50 kHz for 60 s. The acoustic data were processed with a Fourier transform using a window size of 8192 samples (Δt = 164 ms). A Hanning-weighting function with 50% overlap was utilized, resulting in a frequency resolution of about 6 Hz. Conventional frequency domain beamforming [19] was performed on a grid in the range of x/c = [-1, 3] and z/c = [-2, 2]. The grid point resolution is 10 mm. Source Power Integration technique [20] was used assuming the presence of a line noise source located at the airfoil trailing edge. The selected parameters provide adequately high resolution and signal-to-noise ratio across a frequency range of 500 to 5000 Hz. Results were integrated in the range x/c = [0.90, 1.10] and z/c = [-0.33, 0.33]. The sound intensity per unit span obtained using various spanwise extents of integration region is nearly uniform. One example of the source map at 1250 Hz for the freestream velocity of 25 m/s is shown in Fig. 3(b). The noise source at the trailing edge area is identified with high resolution. The integration area is illustrated by the dashed box.

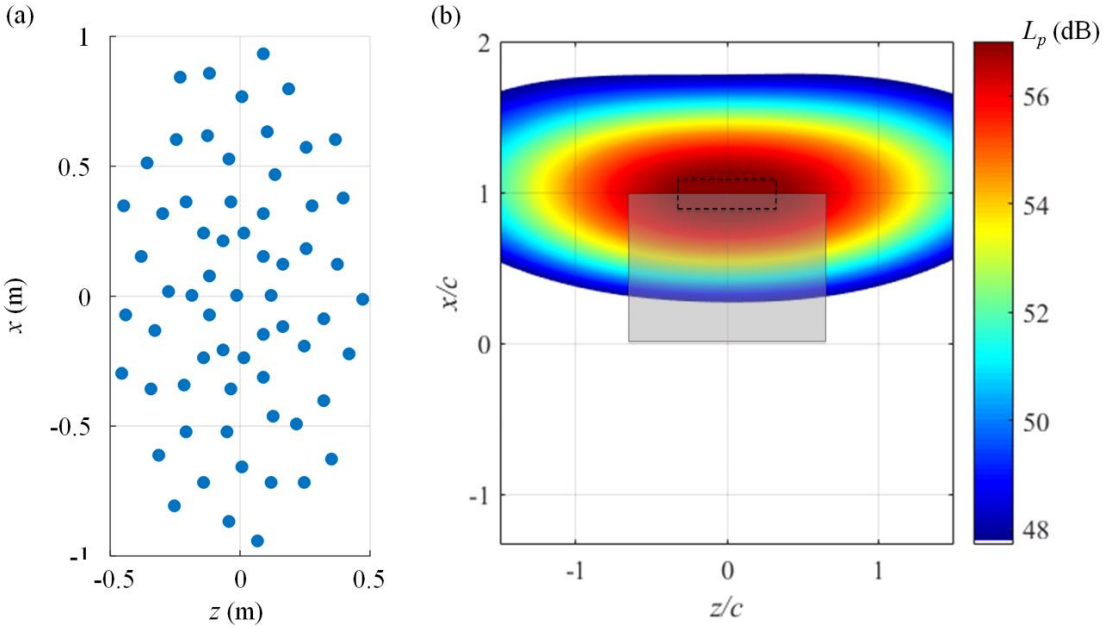

Fig. 3. (a) Arrangement of the microphone array and (b) source map in the x-z plane for the 1/3 octave band with center frequency at 1250 Hz, u_∞ = 25 m/s. In the source map, the airfoil model is shown by the gray area. The dashed box indicates the integration area.

IV. Surface Temperature Distribution

The development of the flow field over the suction side of the airfoil is first described by looking at the surface temperature distributions shown in Fig. 4. The tripping effects of the grit and the zigzag strip at six different freestream velocities (u_∞ = 16, 18, 20, 25, 30, and 35 m/s, respectively) are compared. The onset of laminar to turbulent transition is detected from the decrease in surface temperature caused by the increased level of convective heat transfer downstream of this location. The surface temperature nonuniformity due to preheating is corrected by subtracting the surface temperature with the tunnel off (the absence of the flow).

For $u_\infty \leq 20$ m/s, the grit is observed to be less effective in promoting transition in comparison with the zigzag trip. At u_∞ = 16 m/s, the transition front is at x_t/c = 0.70 for the grit (Fig. 4(a.1)) and is uniform in the spanwise direction. No footprint of flow structures in the near wake of the roughness elements is detected, indicating that the grit is unlikely to influence the transition location. On the other hand, low-temperature regions appear directly downstream of the front facing apexes of the zigzag strip (Fig. 4(b.1)). The intensity of the low-temperature regions decreases farther downstream until transition onset occurs near x_t/c = 0.65, which is slightly upstream of the transition location for the randomly distributed roughness elements. Increasing u_∞ to 18 m/s, the transition front moves slightly upstream to x_t/c = 0.60 for the grit and all the way to x_t/c = 0.26 for the zigzag trip (Fig. 4(a.2) and 4(b.2), respectively). Due to the nonuniform distribution of the grit, two turbulent wedges originate as far upstream as x_t/c = 0.26 near z/c = 0.28 and z/c = -0.18, respectively. A visual inspection indicates that the grit is more densely distributed near these two locations. For the zigzag, additional low-temperature regions with stronger intensity are formed at the transition front. The spanwise locations of the new structures correspond to downstream pointing apexes of the zigzag. At u_∞ = 20 m/s, the transition front moves to x_t/c = 0.25 for both roughness types (Fig. 4(a.3) and (b.3)). Although both trips appear to yield comparable tripping effectiveness at this flow condition, a better spanwise uniformity of the transition front is provided by the zigzag trip.

For u_∞ equal to 25 and 30 m/s (Fig. 4(a.4)(b.4) and (a.5)(b.5), respectively), the transition front moves even closer to the roughness elements at x_t/c = 0.2 and x_t/c = 0.19, respectively, with good spanwise uniformity for both trips. At the highest u_∞ of 35 m/s (Fig. 4(a.6)(b.6)), transition occurs over the roughness strip for the grit, due to the sensitivity to the roughness elements within the upstream portions of the roughness strip. Conversely, for the zigzag, the transition front is now located at x_t/c = 0.18, which is directly downstream of the zigzag strip. In this case, the disturbances are produced on the shear layer originated from the zigzag [21]. These disturbances are amplified as the shear layer develops downstream. Transition onset is expected to occur when the fluctuation level reaches some critical value. The transition locations for all of the flow conditions are summarized in Table 2.

Table 2. Transition locations behind the grit and zigzag at different flow conditions.

u_∞ (m/s)	16	18	20	25	30	35
Grit (x_t/c)	0.70	0.60	0.25	0.20	0.19	0.14
Zigzag (x_t/c)	0.65	0.26	0.25	0.20	0.19	0.18

V. Near Wake Flow Topology

To further investigate the flow topology in the vicinity of the roughness elements and within their wake, the time-averaged velocity fields are measured via hotwire anemometry at two freestream velocities, u_∞ = 20 m/s and 25 m/s, respectively. Cross-plane contours of root mean square (RMS) of streamwise velocity fluctuations ($\langle u' \rangle / u_\infty$) at four streamwise positions (x/c = [0.16, 0.19, 0.24, 0.29]) are shown for both types of trips in Fig. 5 for u_∞ = 20 m/s and in Fig. 6 for u_∞ = 25 m/s. The contour lines of time-averaged velocity (u/u_∞) are also shown for better interpretation of the velocity fluctuations.

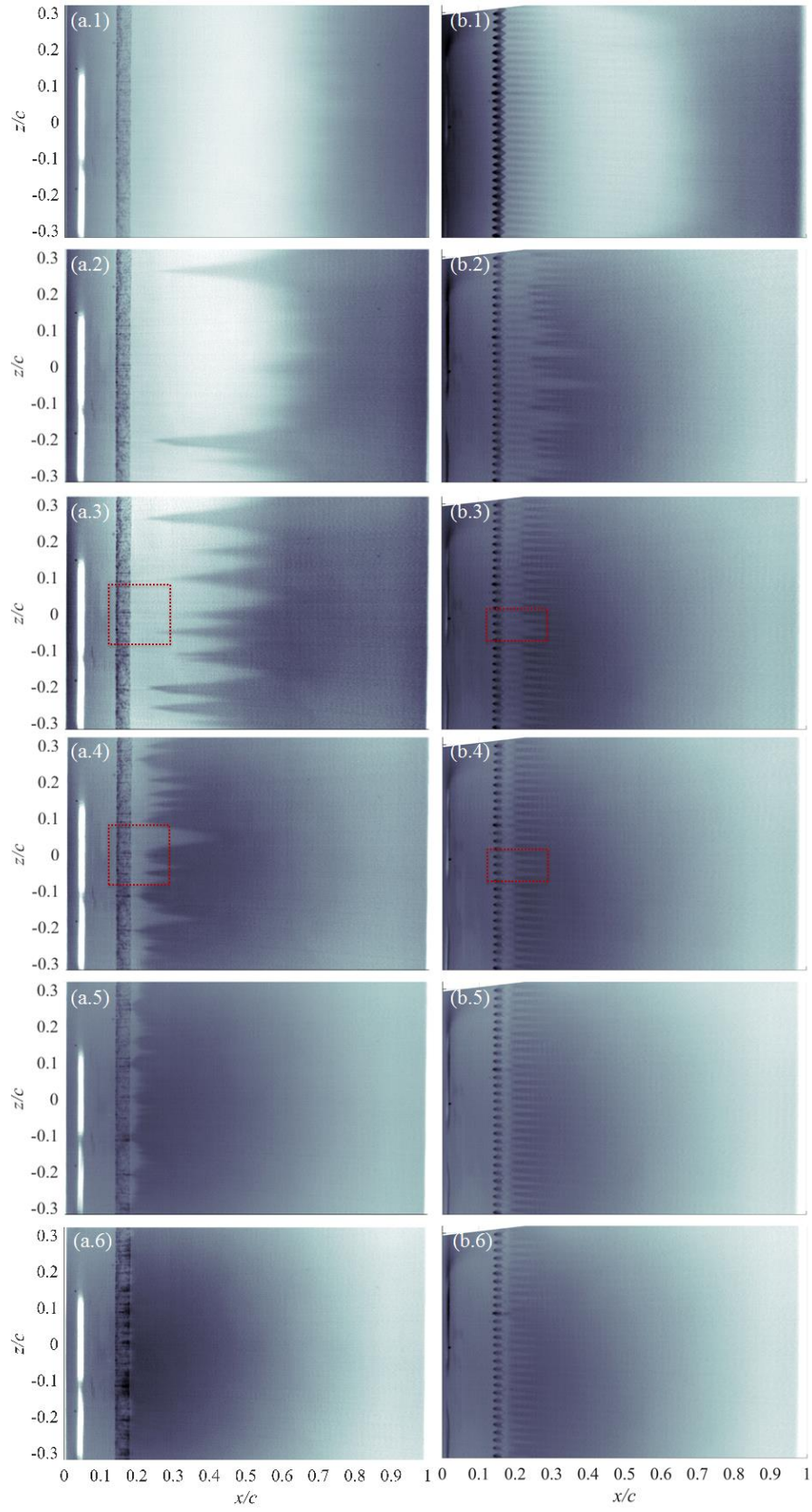

Fig. 4. Surface temperature distribution. (a) and (b) correspond to the grit and zigzag, respectively. (1)-(6) represent u_∞ = 16, 18, 20, 25, 30, and 35 m/s, respectively. The red box indicates hotwire measurement range.

For u_∞ = 20 m/s, an undulated shear flow develops above both roughness configurations at x/c = 0.16 (Fig. 5(a.1) and 5(b.1), respectively). The distribution of velocity fluctuations is uniform along the spanwise direction. The maximum level of velocity fluctuations produced by the zigzag trip is approximately $0.08u_\infty$, which is nearly twice as large as the peak velocity fluctuations due to the grit. At x/c = 0.19 (Fig. 5(a.2)), i.e., slightly downstream of the roughness strip, the undulated shear layer induced by the grit remains uniformly distributed in the spanwise direction, showing no increase of the velocity fluctuation intensity relative to x/c = 0.16. At x/c = 0.24 (Fig. 5(a.3)), a low-speed region of narrow spanwise extent is formed at z/c = -5.33×10^{-2}, which sustains the peak velocity fluctuations at this station. Further downstream, at x/c = 0.29 (Fig. 5(a.4)), this low-speed region expands in the spanwise direction, inducing two more low-speed regions in its vicinity (z/c = -6.00×10^{-2} and -4.67×10^{-2}). The intensity of the velocity fluctuations has further increased to reach a maximum of $0.1u_\infty$ at this station. Two additional locations with secondary local peaks of the velocity fluctuations can be observed at z/c = -1.00×10^{-2} and 8.00×10^{-2}. As found in the surface temperature distribution in Fig. 4(a.3), these locations correspond to the inception of turbulent wedges.

For the zigzag trip, spanwise periodic low- and high-speed regions start emerging at x/c = 0.19 (Fig. 5(b.2)). The locations of the low- and high-speed regions correspond to the downstream and upstream-pointing apexes of the zigzag trip [21]. The higher surface shear stress due to the high-speed regions agrees with the occurrence of low-temperature regions in Fig. 4(b.3). Peaks of velocity fluctuations are produced around the bell-shaped low-speed regions. Further downstream, at x/c = 0.24 (Fig. 5(b.3)), the low-speed regions expand in both wall-normal and spanwise directions, leading to a merger between the neighbouring regions. The intensity of the velocity fluctuations also increases, reaching an average peak level of $0.08u_\infty$. At x/c = 0.29 (Fig. 5(b.4)), the low-speed regions are almost indistinguishable, leading to a relatively uniform region with a high intensity of velocity fluctuations near the wall. A fully turbulent boundary layer is established at this station.

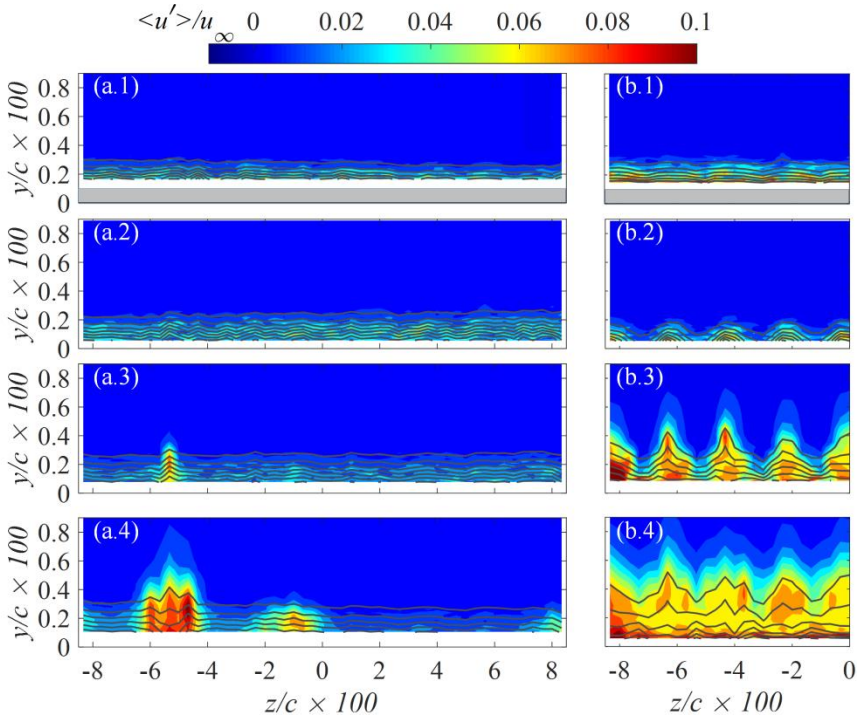

Fig. 5. Cross-plane contours of streamwise velocity fluctuations ($\langle u' \rangle/u_\infty$) on top and downstream of grit (a) and zigzag (b) at u_∞ = 20 m/s. The black lines represent contours of nondimensional time-averaged velocity (u/u_∞) with an increment of 0.1. (1)-(4) correspond to x/c = 0.16, 0.19, 0.24, and 0.29. The y axis is magnified by a factor of 5 for better visualization. The gray area in parts (a.1) and (b.1) indicates the roughness height.

An increase in u_∞ to 25 m/s leads to stronger spanwise modulations above the grit at x/c = 0.16 (Fig. 6(a.1)). The velocity fluctuations are higher in comparison with those seen earlier for u_∞ = 20 m/s. Downstream of the grit at x/c = 0.19 (Fig. 6(a.2)), the stronger mean shear results in a higher intensity of the velocity fluctuations. At x/c = 0.24 (Fig. 6(a.3)), the velocity fluctuations are more uniform in the spanwise direction than for the previous case,

indicating a uniform onset of laminar to turbulent transition. Further downstream at x/c = 0.29 (Fig. 6(a.4)), the flow is completely contaminated by high velocity fluctuations. A fully turbulent boundary layer is found. The flow field around and downstream of the zigzag resembles the one for u_∞ = 20 m/s. The intensity of the velocity fluctuations remains similar at x/c = 0.16 and 0.19 (Fig. 6(b.1)(b.2)). Downstream, at x/c = 0.24 (Fig. 6(b.3)), the active area of low-speed regions undergoes a faster expansion, resulting in a stronger spanwise connection between neighbouring regions. A more homogenous distribution of velocity fluctuations is found at x/c = 0.29 (Fig. 6(b.4)), indicating a fully turbulent boundary layer at this location.

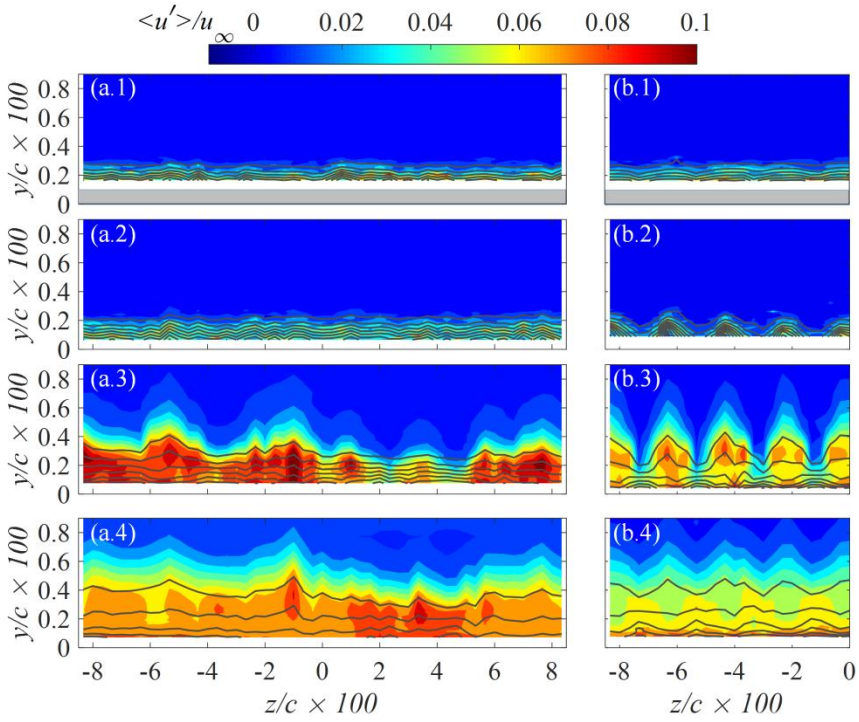

Fig. 6. Cross-plane contours of streamwise velocity fluctuations ($<u'>/u_\infty$) above and downstream of (a) grit and (b) zigzag at u_∞ = 25 m/s. Black lines correspond to contour lines of nondimensional time-averaged velocity (u/u_∞) with an increment of 0.1. (1)-(4) correspond to x/c = 0.16, 0.19, 0.24, and 0.29. The y axis is magnified by a factor of 5 for better visualization. The gray area in parts (a.1) and (b.1) indicates the roughness height.

VI. Flow Properties at the Trailing Edge

The boundary layer near the trailing edge location is characterized with profiles of time-averaged velocity (u/u_∞) and the RMS of the streamwise velocity fluctuations ($<u'>/u_\infty$) at x/c = 0.95 for u_∞ = 20 and 25 m/s, as shown in Fig. 7. The velocity profiles are averaged over the spanwise extent of the measurement domain. The wall-normal positions are normalized with the local boundary layer thickness (δ_{99}). The boundary layer properties for both freestream velocities are summarized in Table 3. When the boundary layer is tripped by the grit and the zigzag strip, the velocity profiles at the trailing edge are almost identical for both cases at the same u_∞, with a peak fluctuation level of around $0.08u_\infty$. The overall shape of the velocity fluctuation profile is analogous to that of a fully turbulent boundary layer [22].

The frequency content of the turbulent fluctuations is investigated through the power spectral density of the streamwise velocity fluctuations at x/c = 0.95, y/δ_{99} = 0.3, as shown Fig. 8. The Kolmogorov's decay law for the inertial subrange [23] is compared with the spectra. The spectra follow the same decay rate as the Kolmogorov law in the frequency range of 200 Hz to 10^4 Hz, confirming the turbulent flow condition at the trailing edge for all the flow conditions considered.

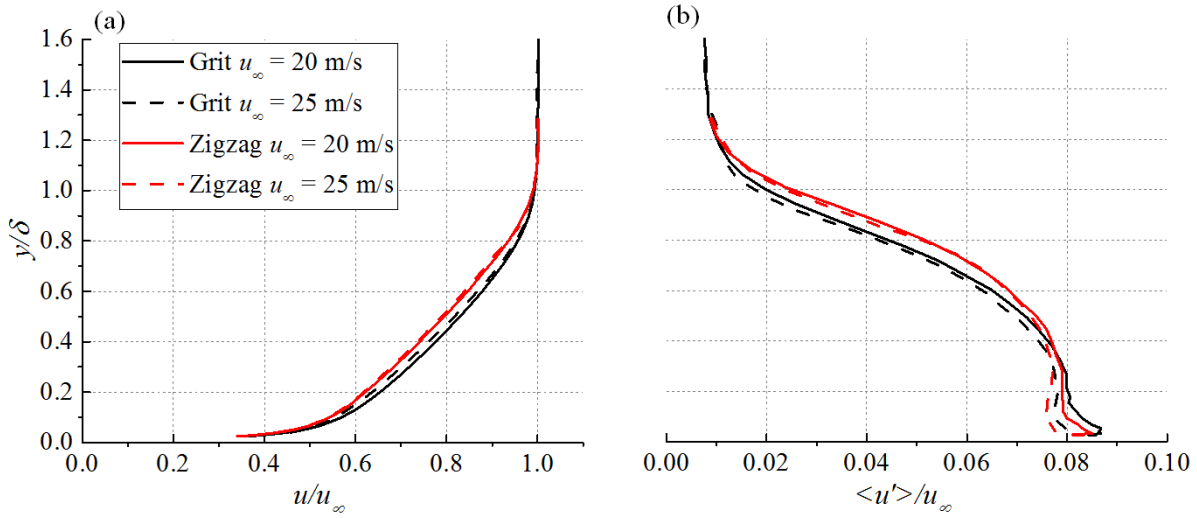

Fig. 7. Profiles of time-averaged streamwise velocity (u/u_∞) (a) and RMS of streamwise velocity fluctuations ($<u'>/u_\infty$) (b) at x/c = 0.95.

Table 3. Model parameters and boundary layer properties at x/c = 0.95 for two selected freetstream velocities. Corresponding parameter values from the experiment of Brooks et al. [12] are shown for comparison.

Roughness type	Grit	Grit	Zigzag	Zigzag	Grit, Brooks et al. [12]
c (m)		0.30			0.30
b (m)		0.40			0.46
R (m)		1.30			1.22
Trip range (x/c)		0.14 - 0.18			0 - 0.2
Trip height (mm)		0.30			0.30
u_∞ (m/s)	20	25	20	25	31.7
M_∞	0.059	0.073	0.059	0.073	0.093
δ_{99} (mm)	7.06	7.45	7.31	6.98	13.5
δ^* (mm)	1.55	1.71	1.72	1.67	3.27
θ (mm)	0.99	1.07	1.08	1.04	1.92
H	1.56	1.60	1.59	1.61	1.70

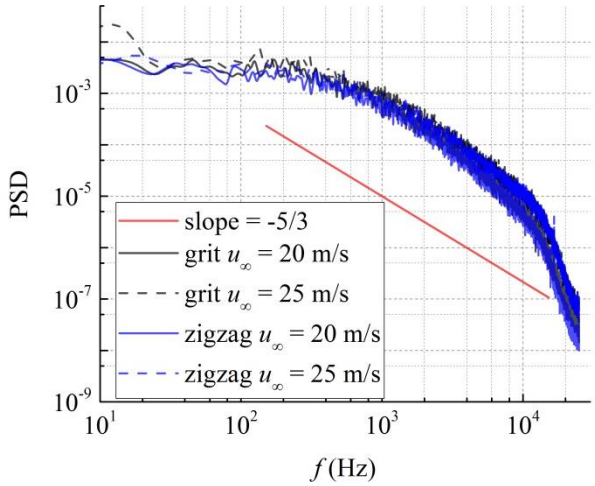

Fig. 8. Power spectral density of the streamwise velocity fluctuations at x/c = 0.95, y/δ_{99} = 0.3.

VII. Far-field Noise

It was shown in the previous section that the boundary layer properties near the trailing edge are very similar for both types of tripping devices. As the trailing edge noise is closely related to the boundary layer thickness at the trailing edge and its spectral content, it is expected that the far-field noise characteristics would also be similar. The farfield noise, expressed in sound pressure level (L_p), for the two tripping devices and six freestream velocities (u_∞ = 16, 18, 20, 25, 30, and 35 m/s) is plotted in Fig. 9. The L_p curves show similar trends for the grit and the zigzag. The sound pressure level grows with an increase in u_∞ as expected (i.e., according to the 5th power law).

The difference between the sound pressure level for the grit and the zigzag cases at each freestream speed is calculated as $\Delta L_p = L_{p,grit} - L_{p,zigzag}$, and is plotted in Fig. 10. ΔL_p depends on both freestream velocity and the frequency parameter. For u_∞ = 16 m/s, the grit produces higher noise level compared with that of the zigzag over the entire range of frequencies measured during the experiment. The maximum ΔL_p of 2.0 dB is found at 2.5 kHz. Increasing u_∞ to 18 and 20 m/s, the noise level of grit is lower for f < 1 kHz while it becomes higher for f > 1 kHz. Maximum noise intensity differences of 2.6 dB and 1.3 dB are observed at 4.0 kHz and 5.0 kHz for u_∞ = 18 m/s and 20 m/s, respectively. A further increase in u_∞ to 25 m/s causes ΔL_p to become negative, indicating that the grit produces lower noise compared with the zigzag, with a maximum ΔL_p of -0.9dB at 4.0 kHz. A similar trend in the ΔL_p spectrum is observed at higher u_∞ of 30 and 35 m/s, with a maximum value of -1.3 dB for both conditions.

In summary, ΔL_p changes from a positive to a negative value across u_∞ = 20 m/s. At lower u_∞, the grit is less effective in promoting boundary layer transition. The flow remains laminar for larger streamwise extent when tripped by the grit. Transition is presumably induced by the growth of two-dimensional TS waves, resulting in a potentially stronger spanwise correlation in the transitional regime in comparison with the correlation across the spanwise periodic flow structures downstream of the zigzag trip. If the higher spanwise correlation were to persist up to the trailing edge, it would lead to an increase in the noise level. The present measurements did not include spanwise correlations near the trailing edge and, hence, the role of spanwise correlation in the reversal of sign in ΔL_p cannot be established at this time. However, we note from Table 3 that the above change in the sign of ΔL_p across u_∞ = 20 m/s is also accompanied by a change in relative boundary layer thickness (albeit a small one) for the distributed roughness elements and the zigzag trip, respectively. The transition fronts for the grit and zigzag exhibit the largest difference at u_∞ = 18 m/s, leading to the highest ΔL_p. The maximum ΔL_p levels are summarized in Table 4.

Table 4. Maximum sound pressure level difference (ΔL_p) and corresponding frequency (f) at different flow conditions.

u_∞ (m/s)	16	18	20	25	30	35
ΔL_p (dB)	2.0	2.6	1.3	-0.9	-1.3	-1.3
f (kHz)	2.5	4.0	5.0	4.0	4.0	4.0

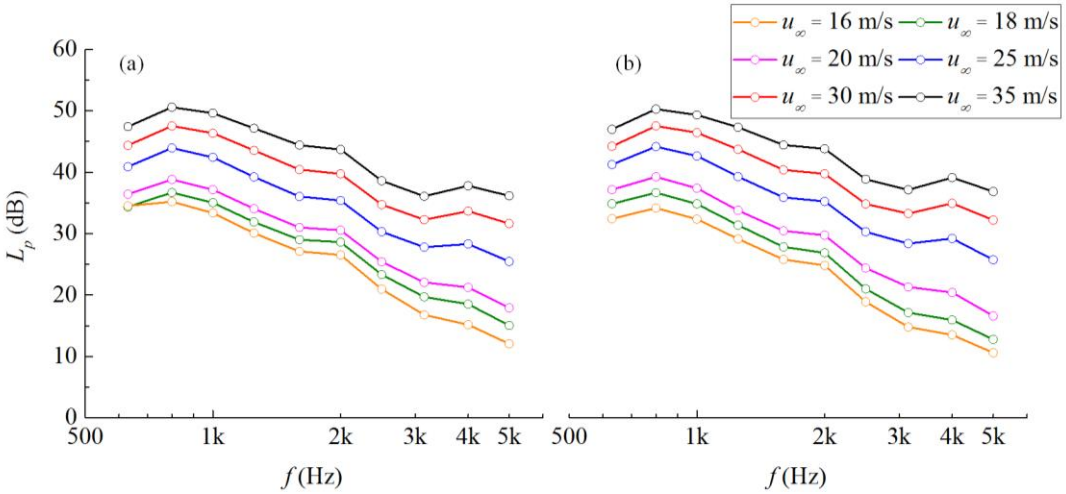

Fig. 9. Sound pressure level L_p when the boundary layer is tripped by (a) the grit and (b) the zigzag at different freestream velocities.

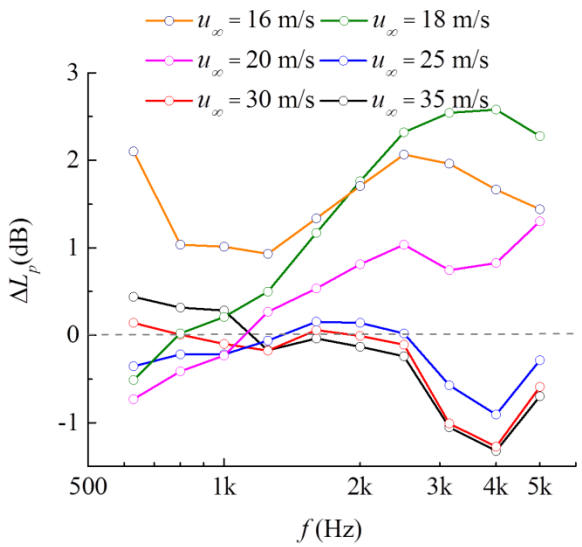

Fig. 10. Sound pressure level difference (ΔL_p) between the grit and the zigzag.

Brooks et al. [12] characterized the trailing edge noise for the NACA 0012 airfoil. Grit particles of the same size were used to force transition; however, the grit was applied over a significantly larger region (from the leading edge until 0.2c on both sides of the airfoil). The experimental results of Brooks et al. [12] are compared with the current dataset. Due to the differences in model span, flow conditions, and microphone arrangement in the two experiments, the sound pressure level is scaled with the Mach number (M_∞), reference observer distance (R), model span (b), and the displacement thickness (δ^*) at x/c = 0.95 [12]:

$$L_{p,norm} = L_p - 50\log(M_\infty) - 10\log(b) - 10\log(\delta^*) + 20\log(R). \quad (1)$$

The parameters for both experiments are summarized in Table 3. The normalized sound pressure level $L_{p,norm}$ is plotted against the Strouhal number St ($St = f\delta^*/u_\infty$) in Fig. 11.

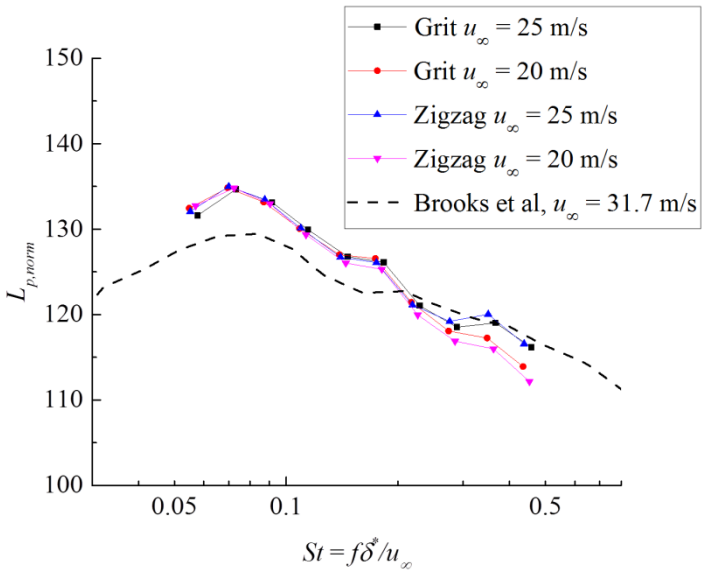

Fig. 11. Normalized sound pressure level ($L_{p,norm}$) compared with Brooks et al. [12].

Two humps present in the spectra at St = 0.07 and 0.18 are due to source noncompactness [24]. A good agreement can be observed with the measurements of Brooks et al. [12] when St > 0.1, with a discrepancy of less than 3.5 dB. For lower St, the spectra deviate from the earlier measurements, yielding a higher discrepancy of up to 5 dB. The exact cause for this disparity remains to be determined; however, it could be related to the differences in tripping configurations. In particular, the boundary layer is likely to have been heavily tripped in the experiment by Brooks et al., leading to a substantially higher boundary layer thickness at the trailing edge in comparison with the present measurements with either type of roughness configuration. A noteworthy observation from Fig. 11 is the excellent collapse for St > 0.1 between the noise spectra for both roughness configurations employed in the present measurements at a fixed freestream speed. This finding indicates that, with due care, the measurements of airfoil trailing edge noise can be rendered nearly insensitive to the details of the trip configuration.

VIII. Conclusions

Laminar to turbulent transition on a NACA 0012 airfoil due to randomly distributed roughness elements, as well as due to a zigzag trip, is investigated experimentally at several freestream velocities. Both roughness types of the same height are placed over the same chordwise extent of the airfoil surface, allowing the effects of both trips on the location of the transition front as well as on the far-field noise characteristics to be compared within a common setting for the first time.

For randomly distributed roughness elements, low-speed regions are formed downstream of the spatial subregions, where the grit is more densely distributed. High levels of velocity fluctuations are produced in these regions, leading to the onset of local turbulent wedges. For a zigzag trip, a spanwise periodic pattern of low-speed regions is generated behind the downstream pointing apexes of the zigzag strip. The spanwise and wall-normal spreading of the low-speed regions leads to interconnection between the neighbouring regions. High intensity velocity fluctuations are produced over the entire span, leading to the onset of transition. The wake of the distributed roughness elements manifests a strong dependence on the local details of the roughness distribution, and this roughness type is found to be less effective in promoting transition than the zigzag trip at low freestream velocity (u_∞ < 20 m/s). When u_∞ is larger than 20 m/s, transition onset occurs across the entire span of airfoil within a narrow range of chordwise stations, causing a rapid upstream shift of the transition front behind the distributed roughness strip and yielding the same or even a slightly upstream transition onset location in comparison with that behind the zigzag trip.

After the establishment of the fully turbulent boundary layer, however, similar boundary layer properties are obtained near the trailing edge for both distributed roughness and the zigzag strip. The far-field noise levels with different surface roughness configurations are closely related to their tripping effectiveness. The noise level for the distributed roughness elements is higher than that of the zigzag trip at u_∞ < 20 m/s. At these flow conditions, transition is induced by the growth of TS waves, and the distributed roughness elements have little influence on the

transition location. The strong spanwise correlation of the two-dimensional TS waves could be responsible for the increased noise level at these lower freestream velocities; however, this conjecture can be neither verified nor refuted due to the limitations of the present measurements. When the transition fronts behind both roughness configurations move to approximately the same chordwise locations at $u_\infty \geq 20$ m/s, the noise level for the distributed roughness becomes lower than that with the zigzag. Compared with the results from Brooks et al. [12], good agreement can be observed when $St > 0.1$. Further analysis of the measurements reported herein is still in progress and their comparisons with the data from Category 1 [2, 25] of the AIAA BANC series of workshops [3] should provide further insights into the observed trends in noise levels as well as clarifying additional details of the transition mechanisms.

Acknowledgments

The authors would like to thank Dr. Roberto Merino Martinez for his support and suggestions on processing the acoustic data.

References

[1] Oerlemans, S., Sijtsma, P., and Méndez López, B., "Location and Quantification of Noise Sources on a Wind Turbine," *Journal of Sound and Vibration*, Vol. 299, No. 4, 2007, pp. 869-883.

[2] Herr, M., Ewert, R., Rautmann, C., Kamruzzaman, M., Bekiropoulos, D., Arina, R., Iob, A., Batten, P., Chakravarthy, S., and Bertagnolio, F. "Broadband Trailing-Edge Noise Predictions: Overview of BANC-III Results," *21st AIAA/CEAS Aeroacoustics Conference*. American Institute of Aeronautics and Astronautics, 2015.

[3] Choudhari, M. M., Bahr, C., Khorrami, M. R., Lockard, D. P., Lopes, L., Zawodny, N., Herr, M., Pott-Pollenske, M., Kamruzzaman, M., Van de Ven, T., Manoha, E., Redonnet, S., Yamamoto, K., Ikeda, I., and Imamura, T., "Simulations & Measurements of Airframe Noise: a BANC Workshops Perspective," Proceedings of NATO STO-MP-AVT-246 Specialists Meeting on Progress and Challenges in Validation Testing for Computational Fluid Dynamics, Avila, Spain, 2016.

[4] Klebanoff, P. S., and Tidstrom, K. D., "Mechanism by Which a Two - Dimensional Roughness Element Induces Boundary-Layer Transition," *Physics of Fluids*, Vol. 15, No. 7, 1972, pp. 1173-1188.

[5] Saric, W. S., Reed, H. L., and Kerschen, E. J., "Boundary-Layer Receptivity to Freestream Disturbances," *Annual Review of Fluid Mechanics*, Vol. 34, No. 1, 2002, pp. 291-319.

[6] Perraud, J., Arnal, D., Seraudie, A., and Tran, D. "Laminar-Turbulent Transition on Aerodynamic Surfaces with Imperfections," *RTO-AVT-111 Symposium*. Prague, Czech Republic, 2004.

[7] Fransson, J. H. M., Brandt, L., Talamelli, A., and Cossu, C., "Experimental and Theoretical Investigation of the Nonmodal Growth of Steady Streaks in a Flat Plate Boundary Layer," *Physics of Fluids*, Vol. 16, No. 10, 2004, pp. 3627-3638.

[8] Joslin, R. D., and Grosch, C. E., "Growth Characteristics Downstream of a Shallow Bump: Computation and Experiment," *Physics of Fluids*, Vol. 7, No. 12, 1995, pp. 3042-3047.

[9] Andersson, P., Brandt, L., Bottaro, A., and Henningson, D. S., "On the Breakdown of Boundary Layer Streaks," *Journal of Fluid Mechanics*, Vol. 428, 2001, pp. 29-60.

[10] Kerho, M. F., and Bragg, M. B., "Airfoil Boundary-Layer Development and Transition with Large Leading-Edge Roughness," *AIAA Journal*, Vol. 35, No. 1, 1997, pp. 75-84.

[11] Hutcheson, F. V., and Brooks, T. F., "Measurement of Trailing Edge Noise Using Directional Array and Coherent Output Power Methods," *International Journal of Aeroacoustics*, Vol. 1, No. 4, 2002, pp. 329-353.

[12] Brooks, T. F., Pope, D. S., and Marcolini, M. A., "Airfoil Self-Noise and Prediction," NASA-RP-1218, 1989.

[13] Cheng, B., Han, Y., Brentner, K. S., Palacios, J., Morris, P. J., Hanson, D., and Kinzel, M., "Surface Roughness Effect on Rotor Broadband Noise," *International Journal of Aeroacoustics*, Vol. 17, No. 4-5, 2018, pp. 438-466.

[14] Sareen, A., Sapre, C. A., and Selig, M. S., "Effects of Leading Edge Erosion on Wind Turbine Blade Performance," *Wind Energy*, Vol. 17, No. 10, 2014, pp. 1531-1542.

[15] van Rooij, R. M., and Timmer, W. A., "Roughness Sensitivity Considerations for Thick Rotor Blade Airfoils," *ASME. J. Sol. Energy Eng.*, Vol. 125, No. 4, 2003, pp. 468-478.

[16] Timmer, W. A., "Two-Dimensional Low-Reynolds Number Wind Tunnel Results for Airfoil NACA 0018," *Wind Engineering*, Vol. 32, No. 6, 2008, pp. 525-537.

[17] Hu, N., and Herr, M. "Characteristics of Wall Pressure Fluctuations for a Flat Plate Turbulent Boundary Layer with Pressure Gradients," *22nd AIAA/CEAS Aeroacoustics Conference*. American Institute of Aeronautics and Astronautics, 2016.

[18] Luesutthiviboon, S., Malgoezar, A., Snellen, M., Sijtsma, P., and Simons, D. "Improving Source Discrimination Performance by Using an Optimized Acoustic Array and Adaptive High-Resolution CLEAN-SC Beamforming," *7th Berlin Beamforming Conference*. Berlin, 2018.
[19] Brandt, A. *Noise and Vibration Analysis: Signal Analysis and Experimental Procedures*. United Kingdom: John Wiley & Sons, 2011.
[20] Merino Martinez, R., Sijtsma, P., and Snellen, M. "Inverse Integration Method for Distributed Sound Sources," *7th Berlin Beamforming Conference*. Berlin, 2018.
[21] Elsinga, G. E., and Westerweel, J., "Tomographic-PIV Measurement of the Flow Around a Zigzag Boundary Layer Trip," *Experiments in Fluids,* Vol. 52, No. 4, 2012, pp. 865-876.
[22] Klebanoff, P. S., Cleveland, W. G., and Tidstrom, K. D., "On the Evolution of a Turbulent Boundary Layer Induced by a Three-Dimensional Roughness Element," *Journal of Fluid Mechanics,* Vol. 237, 1992, pp. 101-187.
[23] Kolmogorov Andrei, N., Levin, V., Hunt Julian Charles, R., Phillips Owen, M., and Williams, D., "The Local Structure of Turbulence in Incompressible Viscous Fluid for Very Large Reynolds Numbers," *Proceedings of the Royal Society of London. Series A: Mathematical and Physical Sciences,* Vol. 434, No. 1890, 1991, pp. 9-13.
[24] Roger, M., and Moreau, S., "Extensions and Limitations of Analytical Airfoil Broadband Noise Models," *International Journal of Aeroacoustics,* Vol. 9, No. 3, 2010, pp. 273-305.
[25] Herr, M., and Kamruzzaman, M. "Benchmarking of Trailing-Edge Noise Computations---Outcome of the BANC-II Workshop," *19th AIAA/CEAS Aeroacoustics Conference*. American Institute of Aeronautics and Astronautics, 2013.